Dalton Transactions

Intrinsic optical bistability and frequency upconversion in Tm3+-Yb3+ codoped Y2WO6 phosphor

Journal:	*Dalton Transactions*
Manuscript ID:	DT-ART-04-2014-001266.R1
Article Type:	Paper
Date Submitted by the Author:	20-Jun-2014
Complete List of Authors:	Vineet Kumar, Rai; Indian School of Mines, Dhanbad, Applied Physics Soni, Abhishek; ISM, Applied Physics

Intrinsic optical bistability and frequency upconversion in Tm^{3+}-Yb^{3+} codoped Y_2WO_6 phosphor

Abhishek Kumar Soni, Vineet Kumar Rai*

Laser and Spectroscopy Laboratory

Department of Applied Physics

Indian School of Mines, Dhanbad-826004

Jharkhand, India

* Authors to whom correspondence to be made:

Email address: vineetkrrai@yahoo.co.in; rai.vk.ap@ismdhanbad.ac.in

Phone No. - +91-0326-2235404

Abstract

The phase and crystal structure of the Tm^{3+}-Yb^{3+} codoped Y_2WO_6 phosphor synthesized through the solid state reaction method has been analyzed by using the X-ray diffraction analysis. The surface morphology and impurity contents present in the phosphor have been analysed by Field emission scanning electron microscopy (FE-SEM) and Fourier transform infrared (FTIR) analysis respectively. The developed phosphor upon excitation at 980nm diode laser radiation shows three upconversion emission bands. The codoping with Yb^{3+} ions in the Y_2WO_6:Tm^{3+} phosphor enhances the frequency upconversion emission intensity significantly. The processes responsible for the UC emissions and their intensity variation upon codoping have been discussed with the help of pump power dependence, energy level diagram and decay curve analysis. The intrinsic optical bistability and colour tunability has also been reported in the developed phosphor.

Keywords*: Phosphor, upconversion, colour coordinate,* intrinsic optical bistability.

1. Introduction

The rare earth (RE) doped phosphors with their multicolour emission properties are extremely used for lighting and display applications [1, 2]. The RE ions contain large number of energy levels and most of them are metastable in nature. From these levels several optical transitions are found by using the suitable excitation wavelength. One of the most attractive properties of RE ions is frequency upconversion (UC), in which the photon of lower energy is converted into the photon of higher energy by means multiphoton absorption or energy transfer mechanism. Rather than the application in display devises, the UC materials are of specific interest to the researchers due to their potential relevance in the optical bio-imaging, enhancement in solar cell energy and temperature sensor [3-5]. In the host materials doped with rare earth ions having lower phonon frequency and non-hygroscopic nature the UC emission efficiency could be enhanced significantly. Fluorides based hosts with lower phonon frequencies have limited applications due to their non-hygroscopic and toxic nature [6]. The oxide hosts due to their high chemical durability, thermal stability, non-toxic nature, non-hygroscopic behaviour and lower phonon frequencies are mostly preferred in several fields [7]. Among the oxide hosts, the Y_2WO_6 is a promising host for making the phosphor materials. Recently, the electronic structure of Y_2WO_6 host shows that it is an indirect band gap material having the band gap 3.13eV and has better electrical conductivity than the Y_2O_3 host [8]. The Tm^{3+} doped phosphors due to their strong blue, near infrared (NIR) and relatively weak red emissions [9] are of great interest to the researchers and technologists among other RE activated phosphors. But the luminescence efficiency in the singly doped materials is relatively low. Therefore, to increase the luminescence efficiency the codoping with lanthanides/non-lanthanides is used. The electronic configuration of Yb^{3+} ion used as a sensitizer is such that the 4f electrons are less shielded than other RE ions therefore, it interacts greatly with the neighbouring ions and lattice [10]. The absorption crosssection

corresponding to the $^2F_{7/2} \rightarrow {}^2F_{5/2}$ transition of the Yb^{3+} ions is higher at the 980nm wavelength and it has the capability to accumulate the excitation energy by absorbing the pump photon. The Yb^{3+} ions, as a sensitizer, transfer their accumulated excitation energy to the nearby activators and hence results the enhancement in the UC emission intensity [11]. It has been found that the optical properties of rare earth doped phosphors depend strongly on their size and morphologies [12]. In order to manage the shape and size of nano-crystalline phosphors many synthesis techniques such as the solid state reaction, co-precipitation, sol-gel, spray pyrolysis, combustion and hydrothermal synthesis have been adopted [13-18]. Among these, the solid state reaction synthesis is a well known distinctive and simple approach for preparation of nano-crystalline RE doped phosphors. The solid state reaction synthesis which occurs at higher temperature is an easy and straightforward synthesis technique having less processing steps and widely used for simple as well as complex inorganic phosphors preparation.

The intrinsic optical bistability (IOB) is one of the special properties of the RE doped materials. Optical bistability (OB) means the hysteresis behaviour observed in the emission intensity versus pump power variation in the nonlinear optical materials. The optical bistable devices have many attractive characteristics and may be used in optical transistor, optical memory, optical gate, optical limiter, etc. [19-22]. For optical data processing, in practice the optical bistable device should be faster and smaller in size, require very little switching energy, consume small amount of energy, and operate at room temperature at a convenient wavelength. The IOB in the lanthanides doped materials has been reported by several researchers [23-27].

In the present paper, for the first time to the best of our knowledge, the UC emissions in the Tm^{3+}-Yb^{3+} codoped Y_2WO_6 phosphor synthesized by the solid state reaction method upon 980nm diode laser excitation has been reported. The information about the crystal

structure, surface morphology and presence of impurity contents in the prepared sample have been analyzed by using the XRD, FE-SEM and FTIR analysis respectively. The effect of codoping with Yb^{3+} ions on the UC emission intensity, pump power dependence and lifetime analysis have been made and the processes involved in the frequency upconversion explored. The colour emitted from the developed phosphor and the phenomenon of intrinsic optical bistability by varying the pump power has been studied.

2. Experimental

2.1. Sample preparation

The Y_2WO_6:Tm^{3+} and Y_2WO_6:Tm^{3+}-Yb^{3+} phosphors have been synthesized by using high temperature solid state reaction method. The raw constituents viz. Tungstates (WO_3), Yttrium oxide (Y_2O_3), Thulium oxide (Tm_2O_3) and Ytterbium oxide (Yb_2O_3) (all 99.9% purity) were taken as the starting materials. A series of samples prepared by the precursor chemicals were taken according to the following compositional equations,

$$(100\text{-}m)\ Y_2WO_6 + n\ Tm_2O_3 \qquad \text{(i)}$$

where m=0.1, 0.2, 0.4, 0.6, 0.8 wt.%.

and

$$(100\text{-}m\text{-}n)\ Y_2WO_6 + m\ Tm_2O_3 + n\ Yb_2O_3 \qquad \text{(ii)}$$

where m=0.4 wt.% and n=0.2, 0.6, 1.0, 2.0, 3.0 wt.%.

During the formation of the host material (Y_2WO_6), the chemical reaction exists itself can be described as,

$$Y_2O_3 + WO_3 \rightarrow Y_2WO_6 \qquad \text{(iii)}$$

The stoichiometric amounts of precursor materials were mixed homogenously with ethanol by using an agate mortar for 20 minutes, and then the mixture was transferred in the alumina crucible, and annealed in a high temperature furnace at 1200^0C temperature for two and half hours. Finally, the annealed samples were used further for all the characterization purposes.

2.2. Measurements and Characterization

All the measurements were carried out at normal room temperature. The X-ray diffraction (XRD) in the range of 10^0-70^0 (2θ degree) of the prepared samples for the crystal structure and phase information has been recorded by X-ray diffractometer. FTIR spectra of the samples have been recorded in the spectral range of 400-4000 cm^{-1}. The surface morphology, particle size and shape of the developed phosphors were examined by using the field emission scanning electron microscopy (FE-SEM). Princeton (Acton SP-2300) monochromator grouped with a photomultiplier tube (PMT) has been used for recording the UC emission spectra upon 980nm continuous wave (CW) diode laser excitation. Lifetime study has been carried out by using the fast signal response digital storage oscilloscope connected with the monochromator.

3. Results and discussion

3.1. XRD study

The XRD pattern of optimized Y_2WO_6:Tm^{3+}-Yb^{3+} phosphor is shown in the Fig. 1. All the peaks are well indexed with the JCPDS file no. 73-0118. This confirms the pure monoclinic phase with space group P2/c of Y_2WO_6:Tm^{3+}-Yb^{3+} phosphor and lattice parameters a = 7.5890Å, b = 5.3340Å, c = 11.3540Å, $\alpha = \gamma = 90^0$ and $\beta = 104^0$, V = 445.15$Å^3$ [28].

The crystallite size of the prepared phosphor has been calculated with the help of XRD peaks broadening estimation by using the following Debye Scherrer's formula [29],

$$l = \frac{0.89\lambda}{\beta_f \cos\theta} \qquad \text{(iv)}$$

where, 'l' is the crystallite size, 'λ' the X-ray wavelength, θ and β_f are the Bragg's angle and full width at half maxima (FWHM) of an estimated peak respectively. The crystallite sizes corresponding to the various planes for the prepared phosphor have been calculated and found in the range of 9 nm to 21 nm. From Table.1, it is clear that the prepared phosphor contains nano-crystalline structures and the crystallite size increases with decrease in the FWHM value of the corresponding planes.

A small amount of lattice strain has been detected due to the mismatch of effective ionic radii of dopant ion (Tm^{3+}, Yb^{3+}) and the replacement site Y^{3+}. The Williamson-Hall (W-H) plot has been used to calculate the crystallite size and lattice strain present in the phosphor. The W-H plot for Y_2WO_6: Tm^{3+}-Yb^{3+} phosphor has been obtained with the following equation [30],

$$\beta_f \cos\theta = 4\varepsilon \sin\theta + \frac{0.89\lambda}{l} \qquad \text{(v)}$$

where, 'ε' is the strain present in the phosphor.

The estimated average crystallite size and lattice strain are found to be ~ 23 nm and ~ 1.35×10^{-2} respectively.

3. 2: FTIR analysis

In the form of impurities present in the prepared phosphor some functional groups have been detected by using the FTIR analysis. The FTIR spectrum of the optimized Y_2WO_6:Tm^{3+}-Yb^{3+} phosphor exhibits the complicated peaks. Strong peak at ~ 434 cm^{-1} attributes as the cut-off

phonon frequency. Therefore, low phonon frequency leads to the minimization of multiphonon relaxation in the prepared phosphor [31]. The tentative functional groups assignments as observed in the FTIR spectrum of prepared phosphor with their vibration frequencies have been shown in the Table. 2.

3. 3: FE-SEM study

The FE-SEM micrograph recorded for the optimized Tm^{3+}-Yb^{3+} codoped Y_2WO_6 phosphor is shown Fig. 2. It is difficult to control the aggregation of particles because the solid state reaction synthesis acquires high temperature rather than a soft chemical rout in which low temperature is needed. From Fig. 2, it is clearly observed that the particles are in agglomerated form with non-uniform size.

3. 4: Upconversion emission study

To optimize the concentration of the dopant ions, concentration versus UC emission intensity has been studied and the graph for the same have been plotted for a series of samples prepared with varying dopant concentrations (Fig. 3). The Tm^{3+} ions are very sensitive during the doping because it has large self quenching at low concentration [32]. For Y_2WO_6:Tm^{3+} phosphor the optimum concentration of Tm^{3+} ions has been found 0.4 wt. % whereas in the case of Y_2WO_6:Tm^{3+}-Yb^{3+} phosphor 0.4 wt.% Tm^{3+}+0.6 wt.% Yb^{3+} combination is optimum. The UC emission intensity starts decreasing on increasing the concentration of Tm^{3+} and Yb^{3+} ions above the optimum value.

The UC emission spectra for the optimized 0.4 wt.% Tm^{3+} doped Y_2WO_6 and 0.4 wt.% Tm^{3+}+0.6 wt.% Yb^{3+} codoped Y_2WO_6 phosphors have been recorded by using 980nm CW diode laser excitation source (Fig. 4). Three bands are observed and assigned, two for visible and one for the near infrared (NIR) region of the electromagnetic spectrum corresponding to

the $^1G_4 \rightarrow {}^3H_6$ (485nm), $^1G_4 \rightarrow {}^3F_4$ (649nm) and $^3H_4 \rightarrow {}^3H_6$ (796nm) transitions respectively. It can be clearly seen from Fig. 4 that the Yb^{3+} ions codoping have no effect on the spectral profile except the intensity variation. The considerable enhancement in all the UC emission bands has been observed due to the codoping with Yb^{3+} ions.

3. 5: Pump Power dependence study and energy level diagram description

On comparing the UC emission spectra profile of the $Y_2WO_6:Tm^{3+}$ and $Y_2WO_6:Tm^{3+}$-Yb^{3+} phosphors, an enhancement around ~260, ~140 and ~164 folds for the blue, red and NIR bands respectively have been detected in the $Y_2WO_6:Tm^{3+}$-Yb^{3+} phosphor compared to the $Y_2WO_6:Tm^{3+}$ phosphor. Such a large enhancement in the UC emission intensity observed from the $Y_2WO_6:Tm^{3+}$-Yb^{3+} phosphor makes the prepared material a superior one with respect to other reported materials [33-36]. The number of NIR pump photons involved in the UC emission process can be identified in a better way by measuring the UC emission intensity as a function of the pump power. This is governed by the following formula,

$$I_{up} \alpha P^{n}_{pump} \qquad \text{(vi)}$$

where, "I_{up}" is the UC emission intensity, "P^{n}_{pump}" is the pump power and "n" is the number of NIR pump photons engaged in the UC emission process [37].

In the case of singly Tm^{3+} doped Y_2WO_6 phosphor the slope values for the logarithmic of pump power versus UC emission intensity are found to be 3.19, 3.35 and 2.31 for 485nm, 649nm and 749nm bands respectively (Fig. 5), while in the Tm^{3+}-Yb^{3+} codoped Y_2WO_6 phosphor the slope values for all the UC emission bands are reduced to 2.19, 1.96 and 2.36 (Fig. 6). This indicates that the upconversion emission bands lying in the blue, red and NIR

region is due to three photons (for blue and red) and two photons (for NIR) absorption. On Yb^{3+} codoping in Y_2WO_6:Tm^{3+} phosphor a reduction in the slope values from three to two for both the UC emission bands at 485nm and 649nm transition is due to the increase in energy transfer rate from Yb^{3+} to Tm^{3+} as well as by the cooperative sensitization process from Yb^{3+}-Yb^{3+}→ Tm^{3+} [38]. Also from Fig. 6, it is clearly observed that at higher pump power reduction in slope value close to one essentially validates the saturation effect. At higher pump power the density of phonons increase which results an increase in the non-radiative relaxation rate and hence the internal temperature of the sample also increases. Due to which the thermalization effect comes into picture and causes no further increase in the UC emission intensity [39].

The energy level diagram of the Tm^{3+}-Yb^{3+} ion system is shown in the Fig. 7. In Tm^{3+} doped phosphor, the UC emission is followed by the non-resonant step wise excited state absorption (ESA) process. The ground state Tm^{3+} ions via non-resonant ground state absorption (GSA) process are pumped to the $^3H_5$ level (~ 2000 cm^{-1}) through non-radiative relaxation. The $^3F_4$ level (~ 2684cm^{-1}) is populated via the non-radiative relaxation from the $^3H_5$ level. The Tm^{3+} ion in the $^3F_4$ level is again promoted to the $^3F_2$ level via the first excited state absorption (ESA-1) process. The population from $^3F_2$ level relaxes non-radiatively to the $^3H_4$ level. The $^3H_4$ level population is again distributed into two ways (i) In populating the $^1G_4$ level via the ESA-2 process (ii) In giving radiative emission corresponding to the $^3H_4$→$^3H_6$ transition peaking at 796nm. Finally, the radiative transition from the $^1G_4$ level to the $^3F_4$ and $^3H_6$ levels emits photons in the red and blue regions respectively. Cooperative sensitization (CS) from Yb^{3+} ions to Tm^{3+} ions has been widely proposed for the Tm^{3+}-Yb^{3+} codoped oxide and fluoride based phosphors [40, 41]. In case of Tm^{3+}-Yb^{3+} codoped system UC dynamics are complex as the incident 980nm photons are absorbed by both the activator (Tm^{3+}) and sensitizer (Yb^{3+}) ions. Most of the upper levels population in Tm^{3+} ion is enhanced by the

energy transfer (ET) from the Yb^{3+} ions to Tm^{3+} ions. The radiative transitions from the different levels in Tm^{3+} ions lead to the UC emissions from the Tm^{3+}-Yb^{3+} codoped Y_2WO_6 phosphor with enhanced intensity compared to that of the Tm^{3+} doped phosphor.

An excited Yb^{3+} ion in the $^2F_{5/2}$ level pumped by the absorption of NIR photon transfers its excitation energy to the Tm^{3+} ion non-resonantly by ET-1 process. The ground state Tm^{3+} ions after absorbing energy from the excited Yb^{3+} ions are promoted to the $^3H_5$ level followed by the emission of five numbers of phonons [42]. Besides this the Yb^{3+} ions have large absorption crosssection and thus absorb 980nm photon efficiently. The $^3H_5$ level of Tm^{3+} ion is depopulated by transferring its population to the $^3F_4$ level. Thus, $^3F_4$ level is populated by nonradiative relaxation from the $^3H_5$ level and the $^3F_2$ level is populated again by the ET-2 process. The population of the $^3F_2$ level is decreased nonradiatively to the $^3H_4$ level via the multiphonon emission. The $^3H_4$ level is depopulated by emitting a NIR photon (796nm) through the $^3H_4 \rightarrow {}^3H_6$ radiative transition. Further, a part of the population from the $^3H_4$ level is promoted to the $^1G_4$ level via the ET-3 energy transfer process from the excited Yb^{3+} ion. The energy difference is again maintained by the emission of four numbers of phonons. A radiative transition from the $^1G_4$ level to the $^3H_6$ and $^3F_4$ level emits the photon in the blue and red regions corresponding to the $^1G_4 \rightarrow {}^3H_6$ and $^1G_4 \rightarrow {}^3F_4$ transition respectively. *D. Li et al.* [43] reported that the blue UC emission corresponding to the $^1G_4 \rightarrow {}^3H_6$ transition is originated due to the two photon absorption process. But in the present case in the singly Tm^{3+} doped phosphor the UC emission band lying in the blue and red region is due to the three NIR photon absorption process (Fig. 5). Therefore, the two photon absorption process in the present case is not responsible for the blue and red emissions. In the codoped phosphor the slope value for the blue and red emission is around ~2, which deviates from the predictable value of ~3. The intensity corresponding to the $^1G_4 \rightarrow {}^3H_6$ transition is large compared to other transitions. Also due to the codoping with Yb^{3+} ions, the UC emission

intensity for all the bands is enhanced by several folds nearly ~260 times for blue, ~140 times for red, ~164 times for NIR bands respectively. The enhancement in the UC emission intensity corresponding to the $^1G_4 \rightarrow {}^3H_6$ transition is large compared to the other transitions. This enhancement is due to the efficient energy transfer from the Yb^{3+} ions to the Tm^{3+} ions. The co-operative energy transfer process from Yb^{3+} to Tm^{3+} ions is also responsible for such a large enhancement in UC emission intensity. In the cooperative energy transfer process the two excited Yb^{3+} ions in the $^2F_{5/2}$ state transfer their energy cooperatively in such a way that one transits upward to a virtual level 'V' and other returns back to its ground state. The excited Yb^{3+} ions in its virtual level transfer their excitation energy to the ground state thulium ions. The ground state thulium ions after receiving this energy are excited to the $^1G_4$ level from where they relax radiatively to different low lying level and gives photons in different regions. Thus the dominant energy transfer process and the probable cooperative energy transfer process from Yb^{3+} to Tm^{3+} are responsible for such a large enhancement. As intensity corresponding to the $^1G_4 \rightarrow {}^3H_6$ transition is ~12 and ~1.89 times higher than the red and NIR bands in Tm^{3+} doped Y_2WO_6 phosphor whereas it is ~23 and ~3 times higher than the red and NIR bands respectively in the codoped phosphor. Therefore, the cross-relaxation process ($^3F_2 + {}^3F_4 \rightarrow {}^3H_6 + {}^1G_4$) along with the aforementioned processes is also responsible for such a large enhancement. The involvement of these processes in the codoped phosphor clearly explains why the slope value is reduced to ~2 from slope value ~3 as observed in the singly doped phosphor.

3. 6: Colour coordinates analysis

In order to get the information about the purity of the colour emitted by the Tm^{3+}-Yb^{3+} codoped Y_2WO_6 phosphor, GoCIE software for colour coordinate calculations has been used at different pump powers {Fig. 8 (a)}. It is clearly seen that the colour coordinates vary from 21mW to 203mW pump power, but for higher pump power ($\leq$ 203mW) the colour

coordinates remain the same. This shows that the colour emitted from the codoped phosphor is tuned from 21mW to 203mW region whereas it does not show the tunability at high pump powers. The blue to red ratio of upconversion emission intensity as a function of pump power has been estimated and observed an increase in the blue to red ratio of upconversion emission intensity up to the 203mW pump power whereas it remains unchanged at higher pump power. This indicates that the developed phosphor can be used in making the low pump power tunable devices and also in making the high pump power display devices. A comparison between the colour coordinate for Tm^{3+}/Tm^{3+}-Yb^{3+} doped/codoped phosphor at 543mW power is shown in the Fig. 8 (b). In the case of codoped phosphor the colour coordinate shifts towards the highly pure blue region and hence the improved blue UC emission is observed upon 980nm diode laser excitation.

3. 7: Decay curve analysis

The decay curve analysis to have a better understanding about the dynamics involved for the improved UC emission intensity enhancement in the codoped phosphor has been done. The decay time by using the decay curve analysis for the $^1G_4$ level in the Tm^{3+}/Tm^{3+}-Yb^{3+} doped /codoped phosphors is calculated and found to be 2.93 ± 0.05ms and 1.15 ± 0.04ms respectively. This decrease in the decay time and hence an increase in the transition probability corresponding to the $^1G_4 \rightarrow {}^3H_6$ transition in the codoped phosphor explains why the UC emission intensity corresponding to the $^1G_4 \rightarrow {}^3H_6$ transition is larger and enhanced significantly due to incorporation of Yb^{3+} ions in the Tm^{3+} doped phosphor.

3. 8: Intrinsic optical bistability (IOB) behaviour

On changing the pump power from 21mW to 1030mW and vice-versa of the Tm^{3+}-Yb^{3+} codoped Y_2WO_6 phosphor, a hysteresis like loop for the $^1G_4 \rightarrow {}^3H_6$ (485nm) and $^3H_4 \rightarrow {}^3H_6$ (796nm) transitions in the pump power range 453mW - 860mW has been observed (Fig. 9).

The presence of the hysteresis loops in the UC emission intensity for a complete cycle range is a good sign of the IOB. *Hehlen et al.* [26, 44] reported the phenomenon of IOB by cooperative energy transfer process in which the two Yb^{3+} ions form the dimer due to the interaction in their excited state. To avoid laser induced heating the excitation power density was kept low. In the present case the excitation power density was 66.9W/cm^2 (for pump power 1030mW) which is smaller than 500W/cm^2 [45]. The dramatic nonlinear phenomenon and room temperature IOB arises due to the strong energy transfer from Yb^{3+} ions to Tm^{3+} ions. Usually, in Tm^{3+}-Yb^{3+} codoped system, the UC mechanism is determined by the cooperative sensitization between the Yb^{3+} to Tm^{3+} ions. The concentration of Tm^{3+} ions in the present case is low compared to the Yb^{3+} ions and hence the cooperative sensitization from Yb^{3+} to Tm^{3+} ions in general is due to the dipole-dipole interaction [46]. Thus, Yb^{3+} ions form a dimer by interaction of Yb^{3+}-Yb^{3+} ions pair in $^2F_{5/2}$ excited state. The origination of the Yb^{3+}-Yb^{3+} ions pair dimer and formation of nanosized cluster is responsible for the typical hysteresis behaviour. Also, the formation of the nanosized cluster in the atomic scale may be playing a dominant role for IOB in the case of Tm^{3+}-Yb^{3+} codoped Y_2WO_6 phosphor. Therefore, hysteresis like loop in the UC emission intensity due to the IOB arises with the pump power variation even at room temperature.

Conclusion

The pure monoclinic phase Y_2WO_6 phosphors codoped with Tm^{3+} and Yb^{3+} ions by conventional solid state reaction synthesis have been synthesized successfully. The significant enhancement in the intensity of UC emission bands arising from Tm^{3+} ions on codoping with Yb^{3+} ions in the developed phosphor has been observed and explained on the basis of energy transfer and cooperative sensitization. The decrement in the slope value (~ 1)

at high pump power has been noted and explained on the basis of saturation effect. The prepared sample emits efficient blue emission and exhibits colour tunability in the low pump power region whereas the colour emitted from the phosphor do not show the colour tunability for higher pump powers. The intrinsic optical bistability and non tunability at higher pump powers in the prepared phosphor makes the material useful is making the optical memory storage, display and other upconversion based optical devices.

Acknowledgements

Authors acknowledge the financial support from University Grant Commission (UGC), New Delhi, India. Mr. Abhishek Kumar Soni is also very much thankful to Indian School of Mines, Dhanbad, India for providing the financial assistance.

References

[1] J. Grube, G. Doke, M. Voss, A. Sarakovskis, M. Springis, Mater. Sci. Eng., 23 (2011) 012004.

[2] K. V. R. Murthy, Rec. Res. Sci. Tech., 4 (2012) 8.

[3] P. Sharma, S. Bropwn, G. Walter, S. Santra, B. Moudgil, Adv. Colloid Interface Sci., 123 (2006) 471.

[4] Y. C. Chen, T. M. Chen, J. Rare Earth, 29 (2011) 723.

[5] A. Pandey, V. K. Rai, Dalton Trans., 4 (2013) 11005.

[6] G. A. Kumar, M. Pokhrel, D. K. Sardar, Mater. Lett., 98 (2013) 63.

[7] T. Li, C. Guo, H. Jiao, L. Li, D. K. Agrawal, Opt. Commun., 312 (2014) 284.

[8] Q. Wang, Z. Ci, G. Zhu, S. Xin, W. Zeng, M. Que, Y. Wang, Opt. Mater. Express, 201460 (2013) 142.

[9] H. K. Yang, B. K. Moon, B. C. Choi, J. H. Jeong, J. H. Kim, K. H. Kim, Solid State Sci., 14 (2012) 236.

[10] L. A. Diaz-Torres, E. De la. Rosa, P. Salas, H. Desirena, Opt. Mater., 27 (2005) 1305.

[11] T. Li, C-F. Guo, Y-M. Yang, L. Li, N. Zhang, Acta Mater., 61 (2013) 7481.

[12] N. Niu, P. Yang, Y. Liu, C. Li, D. Wang, S. Gai, F. He, J. Colloid Interface Sci., 362 (2011) 389.

[13] M. Jiao, Y. Jia, W. Lu, W.Lv, Q. Zhao, B. Shao, H. You, J. Mater. Chem. C, 2 (2014) 90.

[14] W. L. Feng, Y. Jin, Y. Wu, D. F. Li, A. K. Cai, J. Lumin., 134 (2013) 614.

[15] F. Xiao, Y. N. Xue, Q. Y. Zhang, Spectrochim. Acta, Part A, 74 (2009) 758.

[16] S. H. Lee, H. Y. Koo, S. M. Lee, Y. C. Kang, Ceram. Int., 36 (2010) 611.

[17] L. Sun, C. Qian, C. Liao, X. Wang, C. Yan, Solid State Commun., 119 (2001) 393.

[18] T. Grzyb, M. Runowski, A. Szczeszak, S. Lis, J. Solid State Chem., 200 (2013) 76.

[19] J. Y. Gao, J. H. Huang, Z. R. Zheng, Y. Jiang, Y. Zhang, G. X. Jin, Opt. Eng., 34 (1995) 790.

[20] S. L McCall, H. M. Gibbs, T. N. C Venkatesan, J. opt. soc. Am., 65 (1975) 1184.

[21] L. Brzozowski, E. H. Sargent, J. opt. soc. Am. B, 17 (2000) 1360.

[22] B. Ullrich, C. Bouchenaki, S. Roth, Appl. Phys. A, 53 (1991) 539.

[23] Y.-K. Yoon, R. S. Bennink, R. W. Boyd, J. E. Sipe, Opt. Commun., 179 (2000) 577.

[24] A. Kuditcher, M. P. Hehlen, C. M. Florea, K. W. Winick, S.C. Rand, Phys. Rev. Lett., 84 (2000) 1898.

[25] M. P. Hehlen, A. Kuditcher, S. C. Rand, S. R. Luthi, Phys. Rev. Lett., 82 (1999) 3050.

[26] M. P. Hehlen, H. U. Gudel, Q. Shu, J. Rai, S. Rai, S. C. Rand, Phys. Rev. Lett., 73 (1994) 1103.

[27] L. Li, Z. Xin-Lu, C. Li-Xue, Chin. Phys. Lett., 26 (2009) 064216.

[28] M. N. Huang, Y. Y. Ma, F. Xiao, Q. Y. Zhang, Spectrochim. Acta, Part A, 120 (2014) 55.

[29] F. Lei, B. Yan, J. Solid State Chem., 181 (2008) 855.

[30] K. Venkateswarlu, A. C. Bose, N. Rameshbabu, Physica B, 405 (2010) 4256.

[31] J. Dhanaraj, R. Jagannathan, T. R. N. Kutty, C-H. Lu, J. Phys. Chem. B., 105 (2001) 11098.

[32] J. Li, J. Zhang, Z. Hao, X. Zhang, J. Zhao, Y. Luo, J. Appl. Phys., 113 (2013) 223507.

[33] T. A. A. de Assumpção, L. R. P. Kassab, A. S. L. Gomes, C. B. de Araújo, N. U. Wetter, Appl Phys B, 103 (2011) 165.

[34] K. Mishra, N. K. Giri, S. B. Rai, Appl Phys B, 103 (2011) 863.

[35] D. K. Mohanty, V. K. Rai, Y. Dwivedi, Spectrochim. Acta A, 89 (2012) 264.

[36] C. Zhao, X. Kong, X. Liu, L. Tu, F. Wu, Y. Zhang, Kai. Liu, Q. Zeng, H. Zhang, Nanoscale, 5 (2013) 8084.

[37] A. Pandey, V. K. Rai, Appl. Phys. B, 109 (2012) 611.

[38] A. Kumari, V. K. Rai, K. Kumar, Spectrochim. Acta, part A, 127 (2014) 98.

[39] E. Osiac, I. Sokolska, S. Kuck, J. Lumin., 95(2001) 289.

[40] L. Li, H. Lin, X. Zhao, Y. Wang, X. Zhou, C. Ma, X. Wei, J. Alloys Compd., 586 (2014) 555.

[41] M. Misiak, K. Prorok, B. Cichy, A. Bednarkiewicz, W. Strek, Opt. Mater., 35 (2013) 1124.

[42] G. H. Dieke, Spectra and Energy Levels of Rare Earth Ions in Crystals, Interscience Publishers, USA, 1968, pp. 310-313 [ISBN 470 213906].

[43] D. Li, Y. Wang, X. Zhang, K. Yang, L. Liu, Y. Song, Opt. Commun., 285 (2012) 1925.

[44] M. P. Hehlen, H. U. Gudel, Q. Shu, S. C. Rand, J. Chem. Phys., 104 (1996) 1232.

[45] F. Vetrone, R. Naccache, A. Zamarron, A. J. D. L. Fuente, F. Sanz-Rodriguez, L. M. Maestro, E. M. Rodriguez, D. Jaque, J. G. Sole, J. A. Capobianco, ACS Nano, 4 (2010) 3254.

[46] R. Yadav, S. K. Singh, R. K. Verma, S. B. Rai, Chem. Phys. Lett., 599 (2014) 122.

Table caption

Table. 1: Crystallite size corresponding to different planes (h k l) with their FWHM values.

2θ (degree)	cosθ	(h k l)	β_f (FWHM) (in radians)	l(nm)
17.87	0.990	$(\bar{1}02)$	0.0072	19.22
18.92	0.988	(011)	0.0068	20.40
22.86	0.983	(102)	0.0065	21.41
23.62	0.982	(111)	0.0077	18.12
24.49	0.981	(200)	0.0081	17.24
29.36	0.973	$(\bar{1}11)$	0.0095	14.82
29.96	0.972	(013)	0.0087	16.20
32.92	0.966	(202)	0.0102	13.91
33.97	0.964	(020)	0.0085	16.72
35.88	0.960	$(\bar{2}04)$	0.0073	19.58
47.95	0.929	(222)	0.0083	17.77
50.05	0.923	$(\bar{2}04)$	0.0084	17.68
57.98	0.898	(033)	0.0159	9.60
59.84	0.891	$(\bar{4}21)$	0.0161	9.55

Table. 2: Functional group vibration assignments for Y_2WO_6:Tm^{3+}-Yb^{3+} phosphor.

Vibration frequency (cm^{-1})	Functional group vibration assignments
434.57, 491.01	Y-O stretching vibration
592.60, 649.03, 750.62	W-O stretching vibration
840.92, 2364.75	CO_3^{2-} stretching vibration
1371.44	C-O asymmetric stretching vibration
1631.06	O-H bending vibration
2929.13	C-H stretching vibration

Figure caption

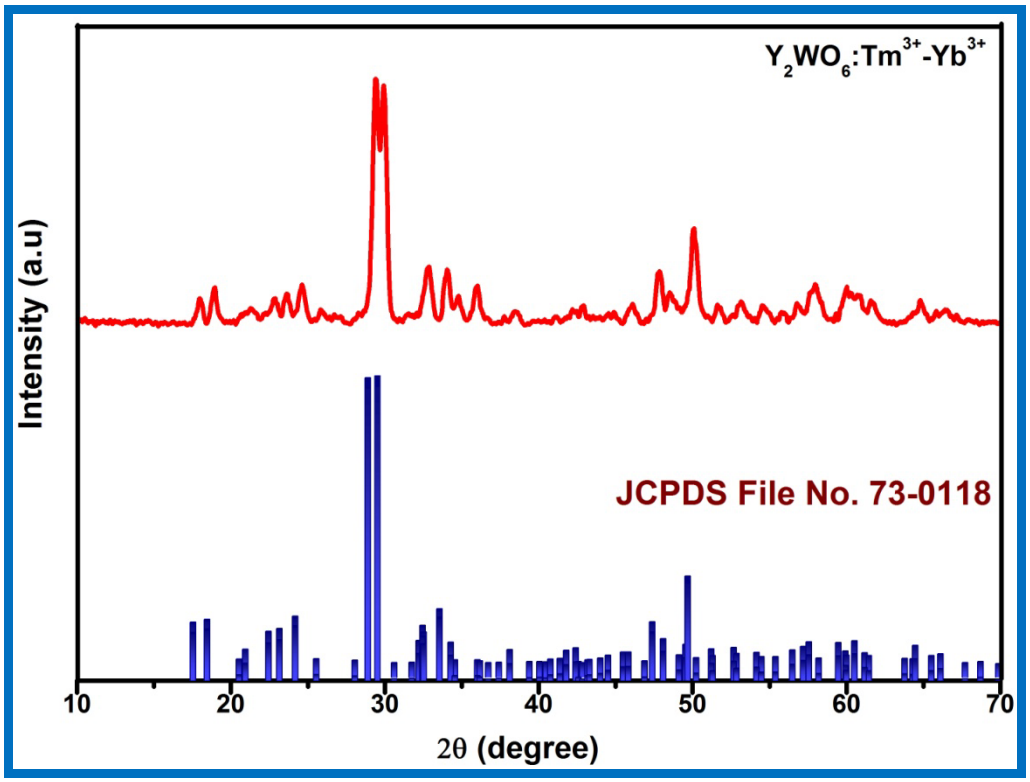

Fig. 1: XRD spectra of $Y_2WO_6:Tm^{3+}$-Yb^{3+} phosphor.

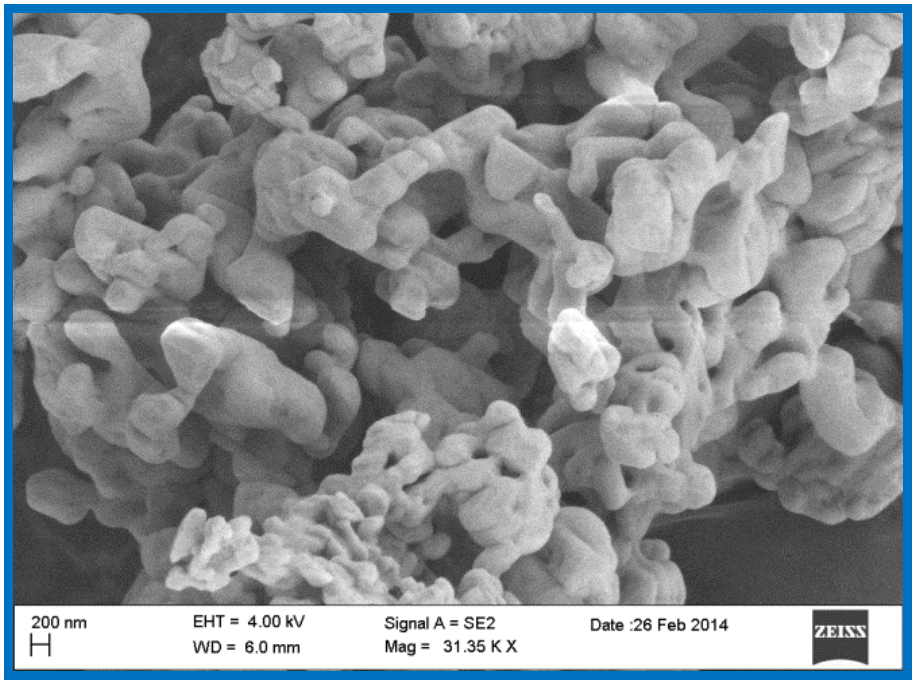

Fig. 2: FE-SEM micrograph of the Y_2WO_6:Tm^{3+}-Yb^{3+} phosphor.

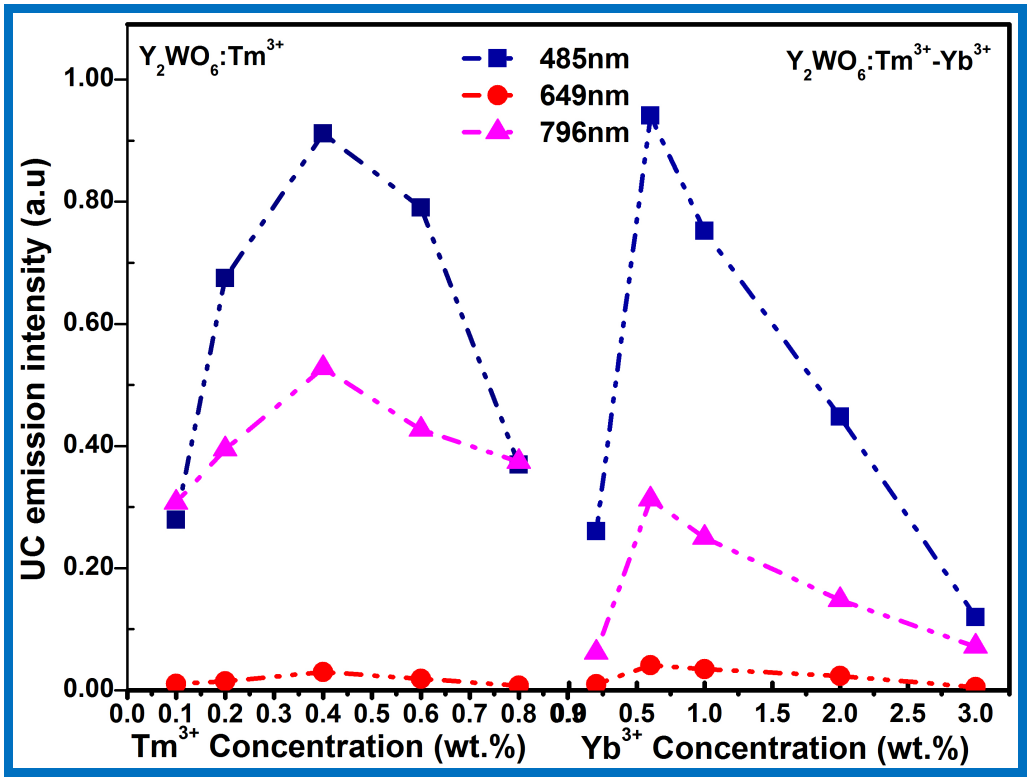

Fig. 3: Concentration dependence of the UC emission intensity (a) $^1G_4 \rightarrow {}^3H_6$ (485nm), (b) $^1G_4 \rightarrow {}^3F_4$ (649nm) and (c) $^3H_4 \rightarrow {}^3H_6$ (796nm) transitions.

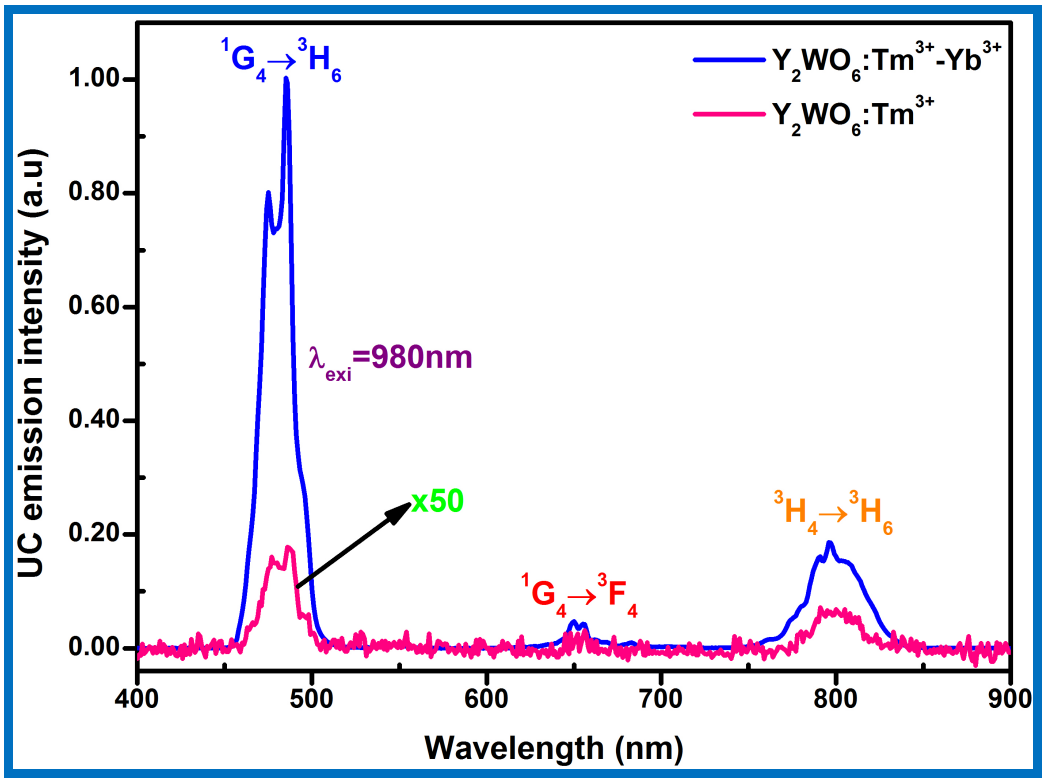

Fig. 4: UC emission spectra of $Y_2WO_6:Tm^{3+}$ and $Y_2WO_6:Tm^{3+}$-Yb^{3+} phosphors.

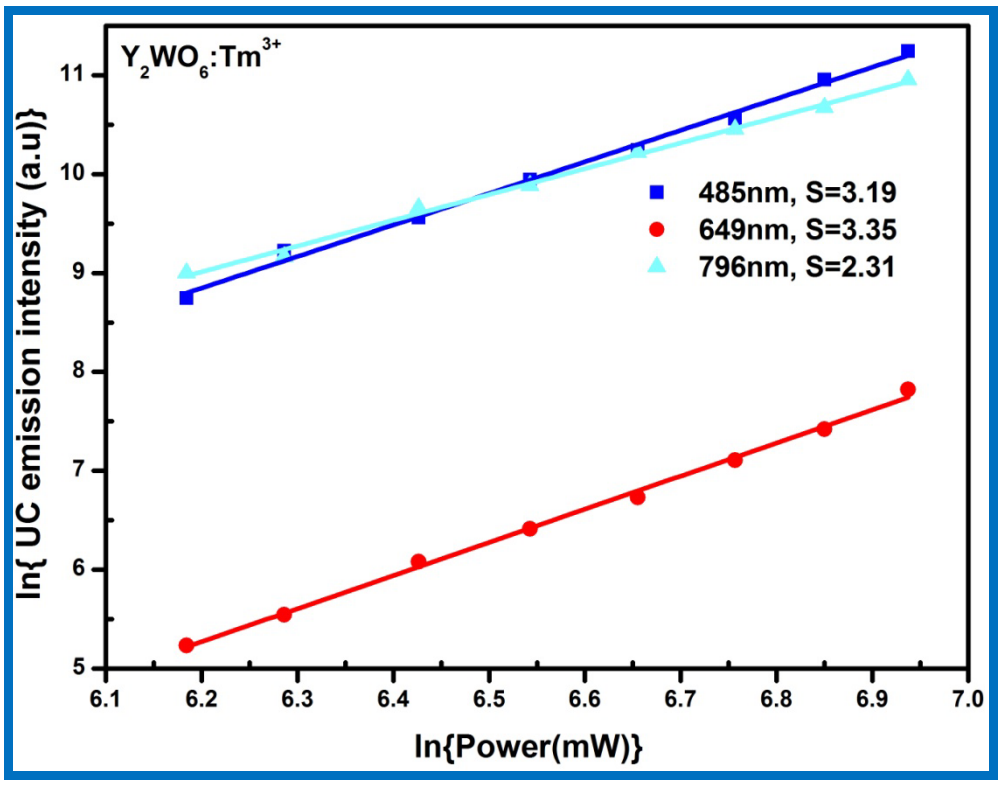

Fig. 5: ln-ln plot for UC emission intensity of the $Y_2WO_6:Tm^{3+}$ phosphor as a function of the pump power.

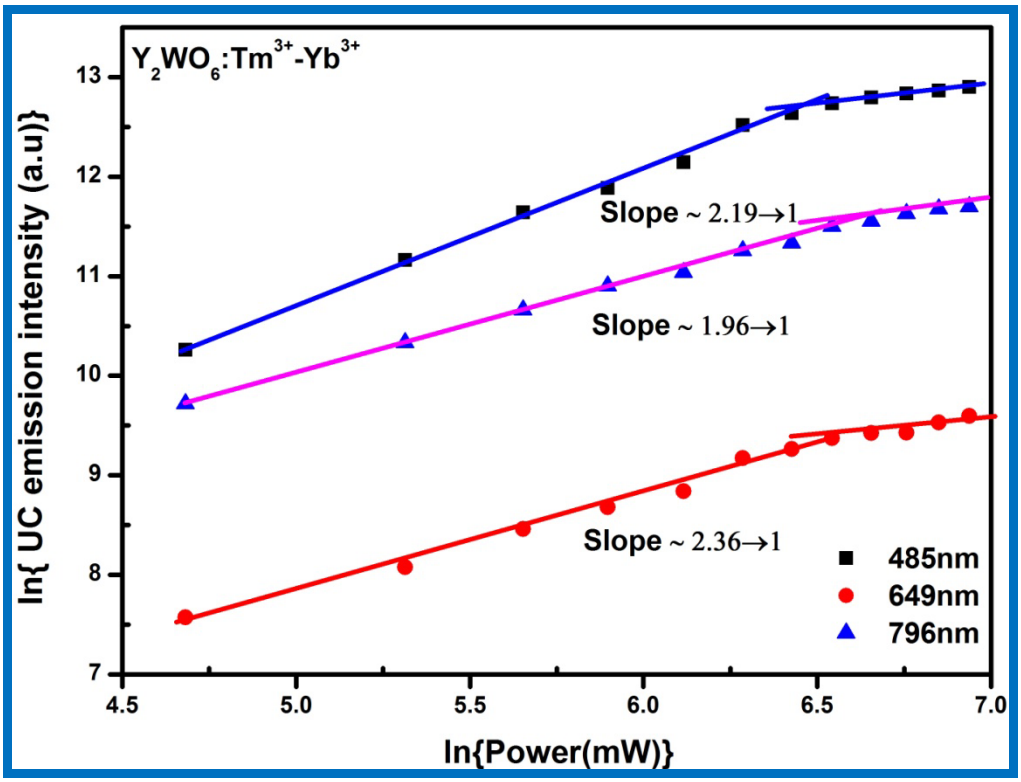

Fig. 6: ln-ln plot for UC emission intensity of the $Y_2WO_6:Tm^{3+}$-Yb^{3+} phosphor as a function of the pump power.

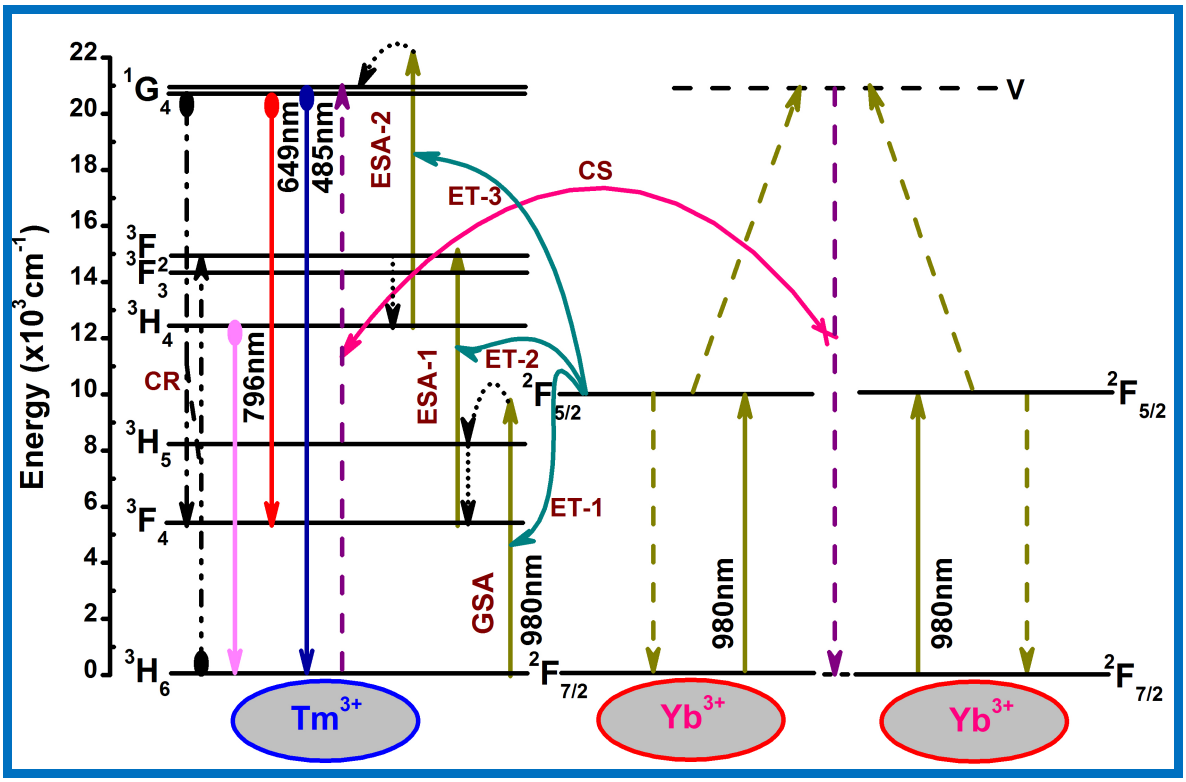

Fig. 7: Proposed schematic energy level diagram of Tm^{3+}-Yb^{3+} codoped Y_2WO_6 phosphor

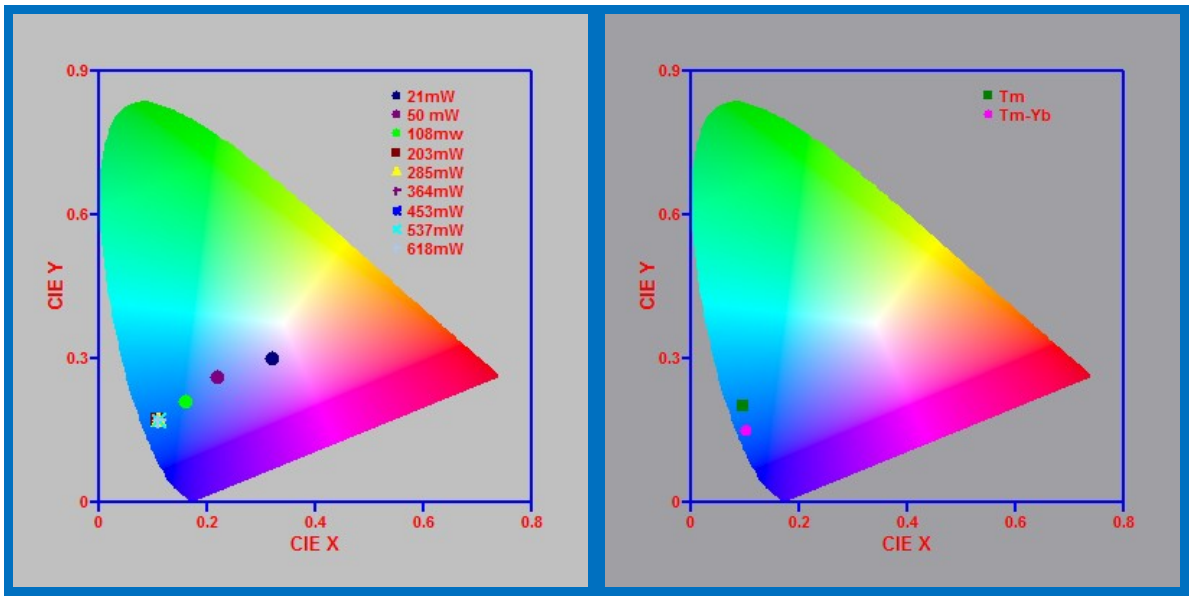

(a) (b)

Fig. 8: (a) Colour coordinates of the Tm^{3+}-Yb^{3+} codoped Y_2WO_6 phosphor at different pump power (b) Colour coordinates for doped and codoped Y_2WO_6 phosphor.

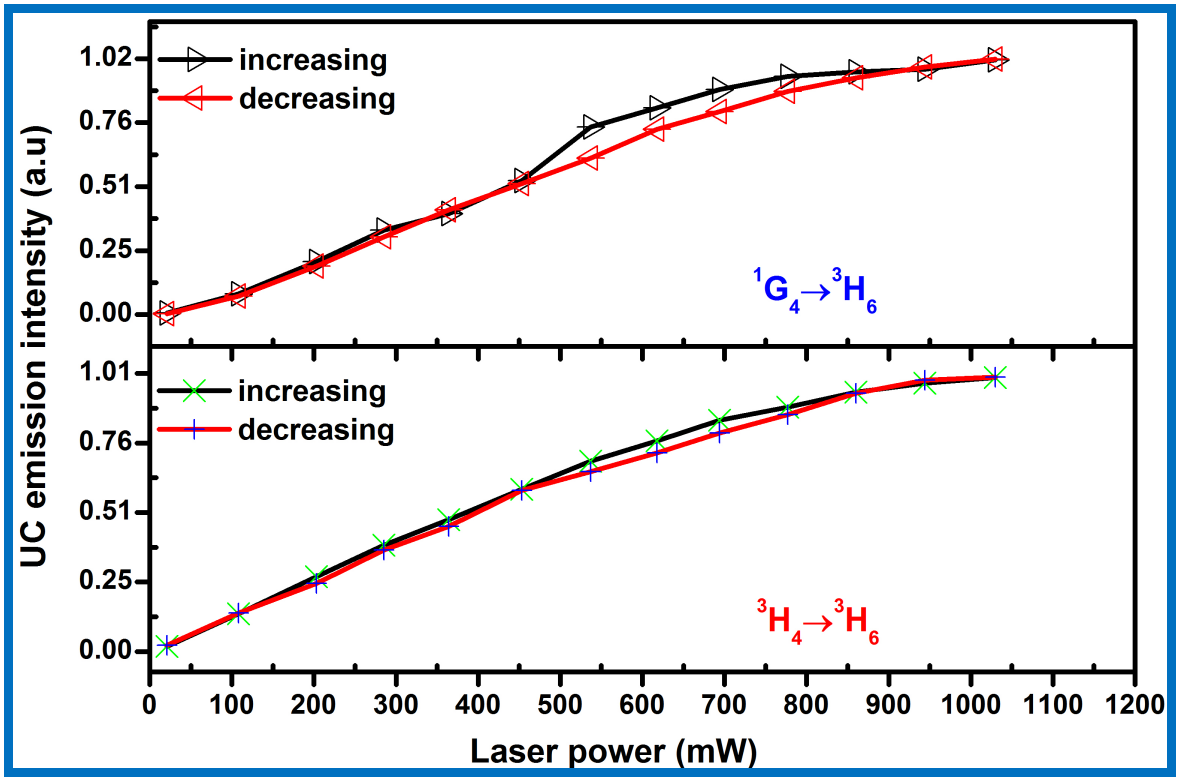

Fig. 9: Intrinsic optical bistability (IOB) behaviour in the Tm^{3+}-Yb^{3+} codoped Y_2WO_6 phosphor.